Low-illumination image denoising method for wide-area search of nighttime sea surface*

SONG Ming-zhu (宋明珠)[1,2], **QU Hong-song** (曲宏松)[1]**, **ZHANG Gui-xiang** (张贵祥)[1], **TAO Shu-ping** (陶淑苹)[1], **and JIN Guang** (金光)[1]

1.Changchun Institute of Optics, Fine Mechanics and Physics, Chinese Academy of Sciences, Changchun 130033, China

2.University of Chinese Academy of Sciences, Beijing 100059, China

(Received 23 December 2017; Revised 24 January 2018)

In order to suppress complex mixing noise in low-illumination images for wide-area search of nighttime sea surface, a model based on total variation (TV) and split Bregman is proposed in this paper. A fidelity term based on L1 norm and a fidelity term based on L2 norm are designed considering the difference between various noise types, and the regularization mixed first-order TV and second-order TV are designed to balance the influence of details information such as texture and edge for sea surface image. The final detection result is obtained by using the high-frequency component solved from L1 norm and the low-frequency component solved from L2 norm through wavelet transform. The experimental results show that the proposed denoising model has perfect denoising performance for artificially degraded and low-illumination images, and the result of image quality assessment index for the denoising image is superior to that of the contrastive models.

Document code: A **Article ID:** 1673-1905(2018)03-0226-6

DOI https://doi.org/10.1007/s11801-018-7268-x

In recent years, the quantum efficiency and the energy response of the back-illuminated sensor are effectively enhanced with the improvement of the sensor manufacturing technology. Visible light cameras have gradually become capable of low-illumination imaging, which has played an important role in the area of wide-area search at night. However, compared with the images acquired in normal environment, the low-illumination images have more obvious noise, which has a serious impact on the target detection and recognition. Therefore, there is an urgent need to design an effective low-illumination image denoising method.

Denoising aims to reduce the influence produced by noise. This issue was widely discussed and a series of methods were proposed after years of study. At present, the image denoising methods include filtering method, partial differential equation method, nonlocal method, etc[1-6]. Although these methods may have a good effect of removing impulsive noise, Gaussian noise or Poisson noise of an image, the denoising effect on the images mixed with multiple noises is mostly limited. In recent years, the total variation (TV) method has been a typical way to restore an image with heavy noise. Typically, TV model formulates image denoising as an inverse problem:

$$f=Hu+n, \tag{1}$$

where f is a measurement image, u is an unknown true image, H is a linear operator denoting, and n is the additive noise.

The most famous approach to restore u is to solve the minimization problem:

$$\min_u R_1(u)+R_2(u). \tag{2}$$

According to different noise types, $R_1(u)$ is the certain data fitting term, and $R_2(u)$ denotes the regularization term.

Numerous improved algorithms based on TV have been proposed aiming at different types of noises, such as impulsive noise, Gaussian noise, Poisson noise, etc. Sutour[4] minimized TV model with a nonlocal data fidelity term. Lanza[7] used parameterized non-convex regularization and induced sparsity of the gradient magnitudes. Lazzaro[8] developed the weighted TV model via an edge driven metric which effectively reduces computation complexity and time. Wang[9] proposed a wavelet frame-based variational model with the ability of preserving key features for Poisson noise removal. Shen[10] introduced nonlocal similarity model in TV in the wavelet domain which can suppress the heavy noise and preserve the details of images. Selesnick[11] proposed a new cost function involving a nonconvex penalty based on

* This work has been supported by the Major Projects of the Ministry of Science and Technology (No.2016YFB0501202), and the Natural Science Foundation of Jilin Province, China (No.20170101164JC).

** E-mail: quhongsong@aliyun.com

the Moreau envelope and it can be implemented using forward-backward splitting. Chen[12] presented the Moreau envelope viewpoint for the L1/TV image denoising model and five variants were proposed which characterize the solutions of the models. However, most denosing methods above depend on signal or high-frequency noise, which are not effective in the application of low-illumination sea image denoising because the noises are mixed and heavy with different frequencies in this condition.

In this paper, for the night wide-area search (search for ships within a large area of the ocean) application, an improved framework based on TV and split Bregman is introduced for image denoising with complex mixed noises, and first-order TV and second-order TV are contained in the regularization term which can hold image information with different detail requirements.

In the normal case of camera imaging, the output noise is not a major factor that affects image quality. However, when the imaging illumination is low, the difference in the magnitude of the noise and background image information decreases as the exposure time increases, and the noise will not be ignored or even cover some of the image information. At that time, the noise can be produced by the interference process in the objective environment, the readout process by the charge coupler, the signal sampling, quantizing and transmitting, etc. According to the characteristics of their dispersion and randomness, the noises can be divided into impulsive noise (random distribution), Poisson noise (Poisson distribution) and Gaussian noise (Gaussian distribution), as shown in Fig.1.

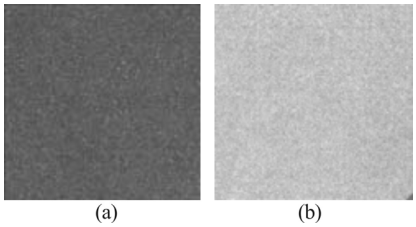

(a) (b)

Fig.1 Imaging effect of GSENSE400 detector in the (a) blackboard and (b) whiteboard (illumination: 0.05 lx, exposure time: 500 ms)

For the terrestrial scene, only impulsive noise is obvious in the case of low illumination because of the rich information of the image, but for the sea surface images, the dark background makes the three kinds of noises more significant. Based on the analysis above, the classic noise model (1) can be expressed as:

$$f(i,j)=\begin{cases} H\,u(i,j)+n_1(i,j) & (i,j)\in\Lambda \\ n_2(i,j) & (i,j)\in\Lambda^c \end{cases}, \tag{3}$$

where Λ is the index set of certain pixel, n_1 represents additive Gaussian noise and Poisson noise on the domain Λ, and n_2 represents the value of impulsive noise on the domain Λ^c.

Eq.(2) is often expressed in the form of the following objective equation for the denoising problem:

$$\min\{\frac{1}{2}\|Hu-f\|_{\omega}+\lambda\times\varphi(u)\}\ , \tag{4}$$

where $\|\ \|_{\omega}$ represents L_{ω} norm. Normally, the fidelity of ω=2 can produce an optimal estimation in the presence of Gaussian noise. The fidelity of ω=1 can suppress the negative impact caused by outliers, but the adverse effect is that most other Gaussian noise pollution data is not suitable. Considering the image in this paper contains a variety of noises, we design the denoising method shown in Fig.2. In this paper, we obtain two images with excessive removal of high frequency and incomplete removal of low frequency through L2 norm and L1 norm design respectively, and the final denoising effect is obtained by mixing and accumulating the high and low frequency information of two images, which can achieve the removal of noise and the preservation of the image details.

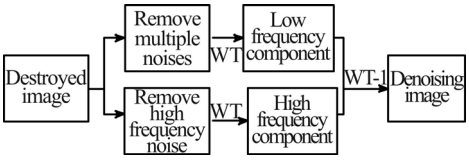

Fig.2 Flow chart of the proposed method

The method is divided into three steps:

Step1. For the removal of all mixed noises. A fidelity term which contains impulsive noise based on L2 norm is designed, and the regularization mixed first-order TV and second-order TV are designed to balance the influence of details information, such as texture and edge for sea surface image. In order to avoid the absorption of high-frequency feature information brought by the introduction of impulse noise term, we adopt a regularization scheme that contains both information to be recovered and additional noise.

The TV model is used to solve the blind image inpainting problem:

$$\min_{u,v}\frac{1}{2}\|u+v-f\|_2^2+\lambda_1\|\nabla u\|_1+\lambda_2\|\nabla^2 u\|_1+\lambda_3\|v\|_1, \tag{5}$$

where f is the observed image, u is the image that is waiting to be recovered, and v is the mixed noises in the observed image. For the variable v, the model of regularization term is restricted to the following assumption that the percentage of impulsive noise is less than a threshold value as Ref.[13], which means that it is sparse on the situation as a whole for one image. λ_1, λ_2 and λ_3 are nonnegative parameters. ∇ is the gradient operator, ∇^2 is the Laplace operator, and they are defined as:

$$\|\nabla u\|_1=\sum\sqrt{|\nabla_x u|^2+|\nabla_y u|^2}\ , \tag{6}$$

$$\|\nabla^2 u\|_1=\sum\sqrt{|\nabla_x{}^T\nabla_x u|^2+|\nabla_y{}^T\nabla_y u|^2}\ . \tag{7}$$

In Eq.(5), it is designed by mixing high and low orders, and L1 module based ∇ operator and ∇^2 operator is selected as a regularization term. The parameters λ_1 and λ_2 are used to balance the weights of the two operators, which can balance the edge effect and the ladder effect in different scenes. But when we have a higher requirement on texture details, adjusting λ is not enough to completely

compensate for the edge loss at that time.

Step2. For the removal of impulsive noise. We design a regularization term based on L1 norm, and the regularization mixed first-order TV and second-order TV are designed as Step1. The TV model is used to solve the blind image inpainting problem at this time:

$$\min_u \|u-f\|_1 + \lambda_1 \|\nabla u\|_1 + \lambda_2 \|\nabla^2 u\|_1 \quad . \tag{8}$$

The parameters in Eq.(8) have the same meanings as Step 1. In Eq.(8), the high-frequency noise and some low-frequency noise are effectively removed, and the image details are effectively preserved.

Step3. We obtain the high and low frequency components L_1, H_1, L_2, H_2 by using the wavelet transform of u_1 and u_2 acquired by Step1 and Step2:

$$[L_1, H_1] = WT(u_1), \ [L_2, H_2] = WT(u_2) \quad . \tag{9}$$

Finally, the inverse wavelet transform is used to synthesize low-frequency components of Step1 and high-frequency components of Step2 to obtain the final denoising image u:

$$u = WT^{-1}(L_1, H_2). \tag{10}$$

The minimization problem can be solved by split Bregman iteration. The split Bregman algorithm was first proposed by Goldstein and Osher in Ref.[14] and it was applied in solving image restoration model based on L1 regularized problem effectively.

We replace ∇u and $\nabla^2 u$ by two new variables d_1 and d_2:

$$d_1 \to \nabla u, \ d_2 \to \nabla^2 u \quad . \tag{11}$$

Eq.(5) can be rewritten as:

$$\min_{u,v} \frac{1}{2}\|u+v-f\|_2^2 + \lambda_1 \|d_1\|_1 + \lambda_2 \|d_2\|_1 + \lambda_3 \|v\|_1 \ ,$$
$$\text{s.t. } d_1 = \nabla u \ , d_2 = \nabla^2 u \ . \tag{12}$$

In order to make Eq.(12) simpler to solve, the constrained optimization problem can be converted into an unconstrained optimization problem:

$$(u^{k+1}, v^{k+1}, d_1^{k+1}, d_2^{k+1}) = \min_{u,v} \frac{1}{2}\|u+v-f\|_2^2 + \lambda_1 \|d_1\|_1 +$$
$$\frac{\gamma_1}{2}\|d_1 - \nabla u - b_1^k\|_2^2 + \lambda_2 \|d_2\|_1 + \frac{\gamma_2}{2}\|d_2 - \nabla^2 u - b_2^k\|_2^2 + \lambda_3 \|v\|_1 . \tag{13}$$

Then we solve the unconstrained optimization problem (13) with the following split Bregman based iterative schemes:

$$\begin{cases} u^{k+1} = \min_u \frac{1}{2}\|u+v^k-f\|_2^2 + \frac{\gamma_1}{2}\|d_1^k - \nabla u - b_1^k\|_2^2 + \frac{\gamma_2}{2}\|d_2^k - \nabla^2 u - b_2^k\|_2^2 \\ v^{k+1} = \min_v \frac{1}{2}\|u^{k+1}+v-f\|_2^2 + \lambda_3 \|v\|_1 \\ d_1^{k+1} = \min_{d_1} \lambda_1 \|d_1\|_1 + \frac{\gamma_1}{2}\|d_1 - \nabla u^{k+1} - b_1^k\|_2^2 \\ d_2^{k+1} = \min_{d_2} \lambda_2 \|d_2\|_1 + \frac{\gamma_2}{2}\|d_2 - \nabla^2 u^{k+1} - b_2^k\|_2^2 \\ b_1^{k+1} = b_1^k + \nabla u^{k+1} - d_1^{k+1} \\ b_2^{k+1} = b_2^k + \nabla^2 u^{k+1} - d_2^{k+1} \end{cases} . \tag{14}$$

Eq.(5) then can be solved with the numerical algorithm below.

In the numerical algorithm above, $\Gamma(\lambda, z)$ is the soft-thresholding operator designed by:

$$\Gamma(\lambda, z) = \text{sgn}(z)\max\{|z| - 1/\lambda, 0\}. \tag{15}$$

Algorithm 1: Numerical algorithm for solving Eq.(5):

(i) Set the initial guesses u^0, v^0, $d_1{}^0$, $d_2{}^0$, $b_1{}^0$, $b_2{}^0$;

(ii) Choose appropriate parameters λ_1, λ_2, λ_3, γ_1, γ_2;

(iii) For k=0,1,… , iterate until convergence.

$$\begin{cases} u^{k+1} = (1+\gamma_1\nabla^T\nabla + \gamma_2(\nabla^2)^T\nabla^2)^{-1}[\gamma_1\nabla^T(d_1^k - b_1^k) + \\ \qquad \gamma_2(\nabla^2)^T(d_2^k - b_2^k) + (f - v^k)] \\ v^{k+1} = \Gamma_{\lambda_3}(f - u^{k+1}) \\ d_1^{k+1} = \Gamma_{\lambda/\gamma_1}(\nabla u^{k+1} + b_1^k) \\ d_2^{k+1} = \Gamma_{\lambda/\gamma_2}(\nabla^2 u^{k+1} + b_2^k) \\ b_1^{k+1} = b_1^k + \nabla u^{k+1} - d_1^{k+1} \\ b_2^{k+1} = b_2^k + \nabla^2 u^{k+1} - d_2^{k+1} \end{cases} . \tag{16}$$

Then, solve Eq.(8). We replace $u-f$, ∇u and $\nabla^2 u$ by three new variables d_1, d_2 and d_3:

$$d_1 \to u - f \ , d_2 \to \nabla u, \ d_3 \to \nabla^2 u \quad . \tag{17}$$

Then Eqs.(12)—(14) can be rewritten as Eqs.(18)—(20):

$$\min_u \|d_1\|_1 + \lambda_1\|d_2\|_1 + \lambda_2\|d_3\|_1 \ \text{ s.t. } d_1 = u - f, d_2 = \nabla u, d_3 = \nabla^2 u \ , \tag{18}$$

$$(u^{k+1}, d_1^{k+1}, d_2^{k+1}, d_3^{k+1}) = \min_u \|d_1\| + \frac{\gamma_1}{2}\|d_1 - u + f - b_1^k\|_2^2 +$$
$$\lambda_1\|d_2\|_1 + \frac{\gamma_2}{2}\|d_2 - \nabla u - b_2^k\|_2^2 + \lambda_2\|d_3\|_1 + \frac{\gamma_3}{2}\|d_3 - \nabla^2 u - b_3^k\|_2^2 , \tag{19}$$

$$\begin{cases} u^{k+1} = \min_u \frac{\gamma_1}{2}\|d_1^k - u + f - b_1^k\|_2^2 + \frac{\gamma_2}{2}\|d_2^k - \nabla u - b_2^k\|_2^2 + \frac{\gamma_3}{2}\|d_3^k - \nabla^2 u - b_3^k\|_2^2 \\ d_1^{k+1} = \min_{d_1} \|d_1\|_1 + \frac{\gamma_1}{2}\|d_1 - u^{k+1} + f - b_1^k\|_2^2 \\ d_2^{k+1} = \min_{d_2} \lambda_1\|d_2\|_1 + \frac{\gamma_2}{2}\|d_2 - \nabla u^{k+1} - b_2^k\|_2^2 \\ d_3^{k+1} = \min_{d_3} \lambda_2\|d_3\|_1 + \frac{\gamma_3}{2}\|d_3 - \nabla^2 u^{k+1} - b_3^k\|_2^2 \\ b_1^{k+1} = b_1^k + u^{k+1} - f - d_1^{k+1} \\ b_2^{k+1} = b_2^k + \nabla u^{k+1} - d_2^{k+1} \\ b_3^{k+1} = b_3^k + \nabla^2 u^{k+1} - d_3^{k+1} \end{cases} . \tag{20}$$

Eq.(8) then can be solved with the numerical algorithm below.

Algorithm2: Numerical algorithm for solving Eq.(8):

(ⅰ) Set the initial guesses u^0, $d_1{}^0$, $d_2{}^0$, $d_3{}^0$, $b_1{}^0$, $b_2{}^0$, $b_3{}^0$;

(ⅱ) Choose appropriate parameters λ_1, λ_2, γ_1, γ_2, γ_3;

(ⅲ) For k=0,1,… , iterate until convergence.

$$\begin{cases} u^{k+1}=(\gamma_1+\gamma_2\nabla^{\mathrm{T}}\nabla+\gamma_3(\nabla^2)^{\mathrm{T}}\nabla^2)^{-1}[\gamma_1(d_1^k+f-b_1^k)+ \\ \quad \gamma_2\nabla^{\mathrm{T}}(d_2^k-b_2^k)+\gamma_3(\nabla^2)^{\mathrm{T}}(d_3^k-b_3^k)] \\ d_1{}^{k+1}=\Gamma_{1/\gamma_1}(u^{k+1}-f+b_1^k) \\ d_2{}^{k+1}=\Gamma_{\lambda_1/\gamma_2}(\nabla u^{k+1}+b_2^k) \\ d_3{}^{k+1}=\Gamma_{\lambda_2/\gamma_3}(\nabla^2 u^{k+1}+b_3^k) \\ b_1{}^{k+1}=b_1^k+u^{k+1}-f-d_1^{k+1} \\ b_2{}^{k+1}=b_2^k+\nabla u^{k+1}-d_2^{k+1} \\ b_3{}^{k+1}=b_3^k+\nabla^2 u^{k+1}-d_3^{k+1} \end{cases} . \tag{21}$$

We examined the performance of the proposed algorithm in comparison with three previous denoising methods generally recognized as effective: block-matching and 3D filtering (BM3D)[3], anisotropic TV denoisng (ATV)[15], non-local means (NLM)[4]. The denoising performance is measured by the peak signal to noise ratio (*PSNR*), and *PSNR* is defined as:

$$PSNR=10\times\log_{10}\frac{MAX^2}{MSE}=20\times\log_{10}\frac{MAX}{MSE} , \tag{22}$$

$$MSE=\frac{1}{mn}\sum_{i=0}^{m-1}\sum_{j=0}^{n-1}\left\|u(i,j)-u'(i,j)\right\|^2 , \tag{23}$$

where *MAX* is the maximum pixel value of the image, u, u' denote the original image and restored image, m and n are the horizontal and vertical pixel numbers, respectively.

In the first experiment, four typical 512×512 images with ship targets (Fig.3) are used as original images in order to examine the denoising performance for signal noise. The four images contain three kinds of standard vessels of hundred meters, ten meters and meters, and cover two application modes including high-resolution target recognition and low-resolution target search, which are well represented in marine target monitoring applications. All the four images are blurred with Gaussian noise, impulsive noise with 0-means and different standard deviation values σ=0.05, 0.10, 0.15 and Poisson noise. The *PSNR* values of restored images with different methods are shown in Tab.1, and Fig.4 shows the examples of restored images.

The second experiment is used to examine the denoising performance for multiple noises. The noise order of low-illumination imaging corresponds to adding mixed Gaussian noise, impulsive noise with 0-means and different standard deviation values σ=0.15 and Poisson noise. In this experiment, the same four typical images above adding multiple noises of low-illumination noise order are used as degraded images. Fig.5 shows the restored images using different methods and their *PSNR* values are shown in a histogram in Fig.6.

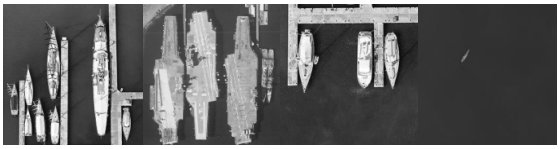

Fig.3 Typical images

Tab.1 *PSNR* (dB) of BM3D, NLM, ATV, OURS for four typical images (signal noise)

Image1			BM3D	NLM	ATV	OURS	Image2			BM3D	NLM	ATV	OURS
Noise	σ	*PSNR*	*PSNR*	*PSNR*	*PSNR*	*PSNR*	Noise	σ	*PSNR*	*PSNR*	*PSNR*	*PSNR*	*PSNR*
	0.05	20.35	23.96	21.99	23.03	**24.04**		0.05	18.65	19.78	20.01	18.60	**20.07**
Gaussian	0.10	20.30	24.05	21.96	23.06	**24.05**	Gaussian	0.10	18.61	19.58	**20.01**	18.37	19.95
	0.15	20.11	**24.12**	21.92	23.14	24.05		0.15	18.54	19.81	20.04	18.69	**20.04**
	0.05	26.40	26.26	26.99	23.53	**27.52**		0.05	19.38	19.77	19.92	18.33	**21.08**
Impulsive	0.10	24.34	24.96	25.66	23.51	**27.84**	Impulsive	0.10	19.01	19.57	18.89	18.10	**20.03**
	0.15	21.33	23.09	23.78	21.58	**26.83**		0.15	18.54	19.16	18.61	18.00	**19.97**
Poisson		25.40	26.26	26.29	23.83	**27.03**	Poisson		18.79	19.41	19.25	18.98	**19.94**
Image3			BM3D	NLM	ATV	OURS	Image4			BM3D	NLM	ATV	OURS
Noise	σ	*PSNR*	*PSNR*	*PSNR*	*PSNR*	*PSNR*	Noise	σ	*PSNR*	*PSNR*	*PSNR*	*PSNR*	*PSNR*
	0.05	20.30	23.90	22.15	23.00	**25.19**		0.05	9.28	9.23	9.00	10.07	**12.27**
Gaussian	0.10	20.27	24.03	22.18	23.39	**25.50**	Gaussian	0.10	9.17	9.21	9.01	9.34	**11.65**
	0.15	20.09	24.43	22.16	23.40	**25.48**		0.15	8.95	8.94	8.89	9.11	**11.53**
	0.05	25.76	26.34	27.70	25.56	**29.67**		0.05	9.90	10.08	9.92	9.87	**13.87**
Impulsive	0.10	24.26	25.53	26.34	24.79	**29.63**	Impulsive	0.10	9.81	10.00	9.79	9.64	**13.95**
	0.15	22.10	24.51	24.28	22.49	**29.61**		0.15	9.42	10.01	9.64	9.41	**13.88**
Poisson		25.76	26.38	26.98	23.86	**27.28**	Poisson		9.28	9.95	9.59	9.81	**12.50**

It can be seen in Tab.1 and Fig.4 that for Gaussian noise and Poisson noise, the results from our method are slightly better than those of BM3D and NLM. For impulsive noise, our method has better performance than other comparison methods obviously. From Fig.5 and Fig.6, we can see that the values of *PSNR* have significant difference and our method is a unique algorithm which can restore images with mixed Gaussian, Poisson and impulsive noises. Though our method has a better *PSNR*, the over-smooth problem still exists and edge details lose in a manner, which forms a constraint for large targets with texture details but a supremacy for small and weak targets.

In the third experiment, an actual remote sensing camera imaging and testing experiment is designed in order to verify the effectiveness of the proposed algorithm. Images above are used as input images shown by the image simulator and a self-developed low-illumination camera (CMOS sensor: GSENSE400) is used in 0.05 lx illumination. The denoising results are shown in Fig.7 and Fig.8. The *PSNR*s of our method are 3.5%, 0.7%, 3.5% and 7.9% higher than those of the best comparison methods for images, respectively.

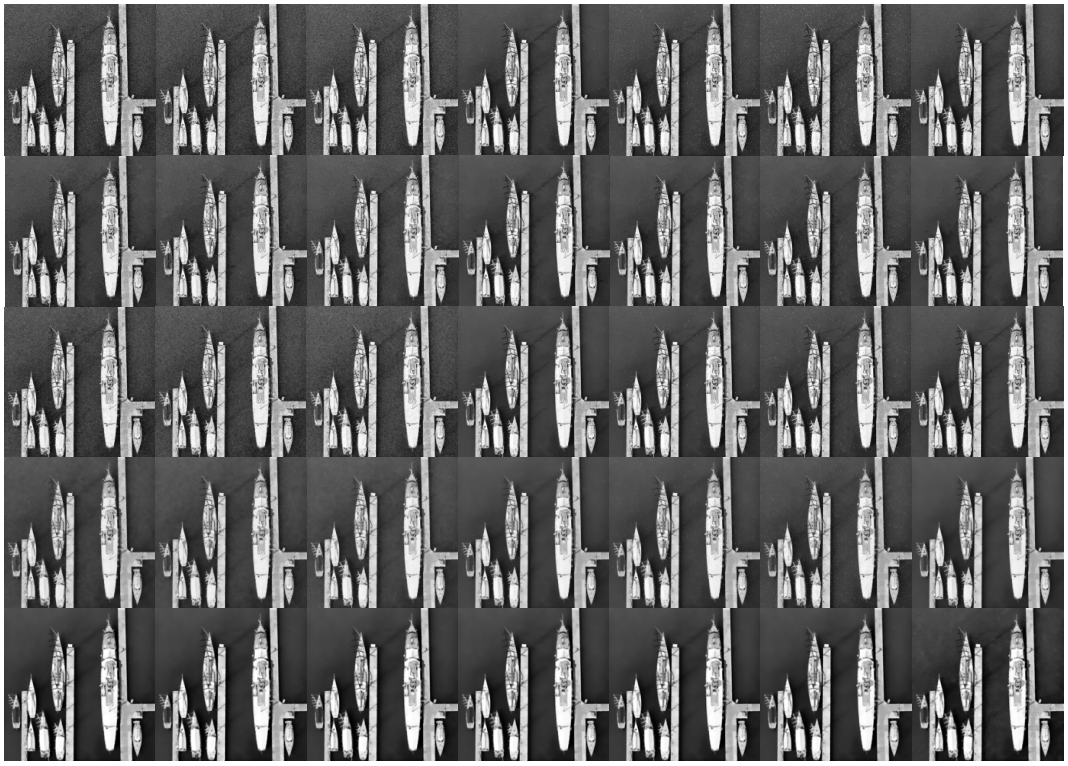

Fig.4 Results on Image1: Top row: Noisy images (From left to right: Gaussian noise (σ=0.05), Gaussian noise (σ=0.10), Gaussian noise (σ=0.15), impulsive noise (σ=0.05), impulsive noise (σ=0.10), impulsive noise (σ=0.15), Poisson noise); Second row: Results by BM3D; Third row: Results by NLM; Fourth row: Results by ATV; Bottom row: Results by the proposed method

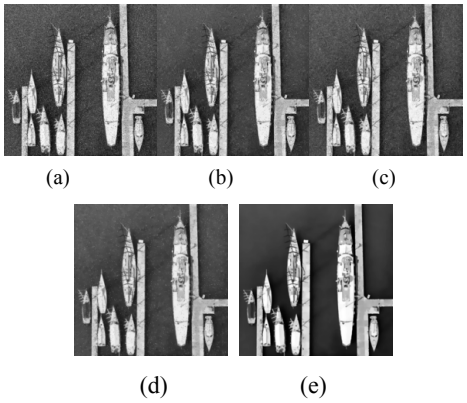

Fig.5 Results on Image1 with multiple noises: (a) Original image; (b) BM3D; (c) NLM; (d) ATV; (e) OURS

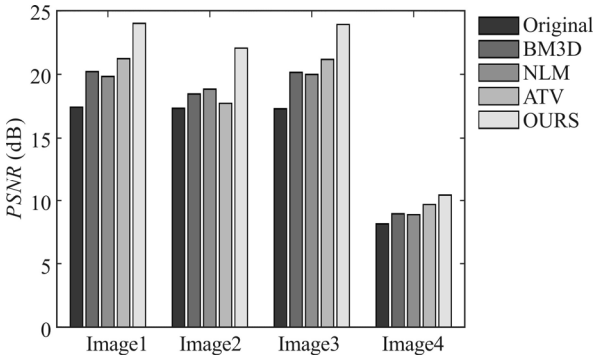

Fig.6 *PSNR* values of comparison methods (multiple noises)

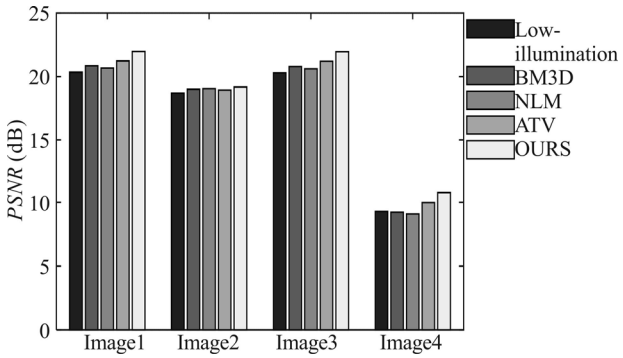

Fig.7 *PSNR* values of comparison methods (low-illumination)

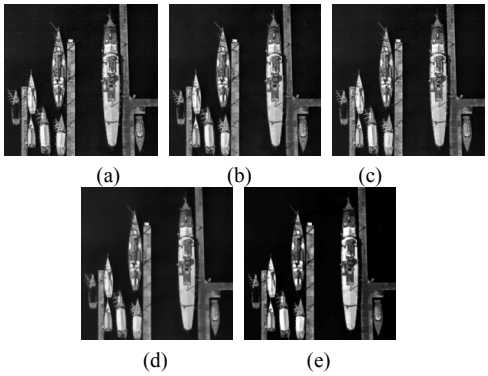

Fig.8 Results on Image1 (low-illumination): (a) Low-illumination image; (b) BM3D; (c) NLM; (d) ATV; (e) OURS

For time consumption experiment, Inter(R) Xeon(R) CPU E5-1620 v2 @3.70 GHz computer and MATLAB R2015a software are used. The average time of our method is 21.33 s, less than 138.5 s (NLM), but more than 11.08 s (ATV) and 13.56 s (BM3D). Time consuming mainly occurs in the iteration of ∇^2 operator. At the same time, it can effectively reduce the time consuming by controlling the iterative accuracy under the premise of ignoring certain denoising accuracy.

In this paper, a method based on TV and split Bregman is proposed to solve the image denoising problem with multiple noises in low-illumination imaging scene. It is shown in the experiments that our algorithm is better than the existing algorithms both in signal noise condition and multiple noise condition, and it has effective application in low-illumination sea image denoising problem. In the future, we will generalize the proposed denoising model to more complicated noise status.

References

[1] V Papyan and M Elad, IEEE Transactions on Image Processing **25**, 249 (2016).

[2] M. Saha, M.K. Naskar and B.N. Chatterji, IETE J. Res **61**,186 (2015).

[3] Kostadin Dabov, Alessandro Foi, Vladimir Katkovnik and Karen Egiazarian, IEEE Transactions on Image Processing **16**, 2082 (2007).

[4] C. Sutour, C.A. Deledalle and J.-F. Aujol, IEEE Transactions on Image Processing **23**, 3506 (2014).

[5] E Luo, S Chan and T Nguyen, IEEE Transactions on Image Processing **24**, 2167 (2015).

[6] K Kasahara, M Shirota and K Kinoshita, Journal of Mathematical Imaging & Vision **56**, 1 (2016).

[7] A. Lanza, S. Morigi and F. Sgallari, J. Math. Imaging Vis **52**, 195 (2016).

[8] Damiana Lazzaro, Applied Mathematics and Computation **297**, 61 (2017).

[9] Cong Wang and Jianbin Wang, Visual Computer, 1 (2017).

[10] Yan Shen, Qing Liu, Shuqin Lou and Ya-Li Hou, IEEE Signal Processing Letters **24**, 877 (2017).

[11] I Selesnick, IEEE Signal Processing Letters **24**, 216 (2017).

[12] F Chen, L Shen, Y Xu and X Zeng, Inverse Problems & Imaging **8**, 53 (2017).

[13] Bin Dong, Hui Ji, Jia Li, Zuowei Shen and Yuhong Xu, Applied and Computational Harmonic Analysis **32**, 268 (2012).

[14] T. Goldstein and S. Osher, SIAM J. Imaging Sci. **2**, 32 (2009).

[15] Y Lou, T Zeng, S. Osher and J Xin, SIAM J. Imaging Sci. **8**, 1798 (2015).